Published in final edited form as:
Curr Biol. 2012 November 6; 22(21): 2081–2085. doi:10.1016/j.cub.2012.09.014.

The retinotopic organization of striate cortex is well predicted by surface topology

Noah C. Benson[1,2,†], **Omar H. Butt**[1,†], **Ritobrato Datta**[1], **Petya D. Radoeva**[1], **David H. Brainard**[2], and **Geoffrey Karl Aguirre**[1,*]

[1]Department of Neurology, University of Pennsylvania, Philadelphia, PA 19104

[2]Department of Psychology, University of Pennsylvania, Philadelphia, PA 19104

Summary

In 1918, Gordon Holmes combined observations of visual field scotomas across brain lesioned soldiers to produce a schematic map of the projection of the visual field upon the striate cortex [1]. One limit to the precision of his result, and the mapping of anatomy to retinotopy generally, is the substantial individual variation in the size [2,3], volumetric position [4], and cortical magnification [5] of area V1. When viewed within the context of the curvature of the cortical surface, however, the boundaries of striate cortex fall at a consistent location across individuals [6]. We asked if the surface topology of the human brain can be used to accurately predict the internal, retinotopic function of striate cortex as well. We used fMRI to measure polar angle and eccentricity in 25 participants and combined their maps within a left-right, transform-symmetric representation of the cortical surface [7]. These data were then fit using a deterministic, algebraic model of visual field representation [8]. We found that an anatomical image alone can be used to predict the retinotopic organization of striate cortex for an individual as accurately as 10–25 minutes of functional mapping. This indicates tight developmental linkage of structure and function within a primary, sensory cortical area.

Results

We obtained retinotopic mapping (RM) data for the central 10° of visual field from 19 participants and the central 20° from a separate group of 6 participants. Voxel-wise polar angle and eccentricity were determined using population receptive field (pRF) methods [9]. Spatially unsmoothed data were combined across hemispheres and subjects within a left-right symmetric, spherical atlas of sulcal topology [7, 10]. Figure 1A illustrates the transformation of polar angle data from the initial pial representation for one subject to the template cortical sphere. Analyses of retinotopic organization were conducted within a region predicted by cortical topology to contain striate cortex [6] (Fig. 1B). We developed an automatic and deterministic algorithm for fitting a retinotopic model to anatomically defined area V1 in the absence of user input (see Methods). We then asked if the RM data

*Correspondence: aguirreg@mail.med.upenn.edu.
†These authors contributed equally to this work

Supplemental Information
Supplemental Information includes 3 figures, Supplemental Experimental Procedures, and a *Mathematica* notebook. Additional data and templates available from https://cfn.upenn.edu/aguirre/wiki/public:data_currbio_2012_benson

from a group could be used to predict the RM of an individual given only an anatomical brain image.

Anatomical prediction of polar angle

Representation of polar angle has been found to correspond to the gyral and sulcal curvature of the cortical surface [11]. When aligned using sulcal topology as a guide, the average polar angle representation across subjects from the 10° dataset (Fig. 2A) demonstrates this relationship and confirms the accuracy of the anatomically defined borders of V1 [6]. At the posterior extent of V1, the measured polar angle representation becomes disorganized as multiple lines of azimuth intersect within the foveal confluence [12].

The aggregate polar angle data were compared to an algebraic template fit to the polar angle data of all subjects in the 10° dataset (Fig. 2B; see Supplemental Materials for details). This template performed nearly uniformly over the extent of V1 for which retinotopic mapping data were available (Fig. 2C).

We next asked how well the retinotopic template generated using our procedure could predict the measured polar angle for an individual. For each subject, a template to which they were compared was constructed using data from all other subjects in a leave-one-out fashion. This template was then used to predict the spatially unsmoothed polar angle organization of the excluded subject, guided only by that subject's cortical anatomy. Figure 2D shows the median absolute error across subjects for the prediction of polar angle along iso-angular bands defined by the template. The median absolute error in the prediction of polar angle was below 12° when aggregated across subjects in a leave-one-out fashion (median absolute and signed errors across all vertices in V1 were 11.43° and -0.93° respectively for leave-one-out comparisons).

Finally, we confirmed that the polar angle fits derived from one group of subjects generalized to a second group. The polar angle fit to the aggregate of data from the 10° dataset (Fig. 2E) matched the fit to the aggregate data from subjects in the 20° dataset (Fig. 2F).

Anatomical prediction of eccentricity

The unsmoothed eccentricity measurements from 19 subjects, studied with RM stimulation out to 10°, were combined (Fig. 3A). An area of low-eccentricity values can be seen extending posteriorly beyond the predicted border of area V1, corresponding to the foveal confluence.

The aggregate eccentricity data were fit with an exponential template (Fig. 3B). Only those points with an assigned eccentricity below 8° and above 2.5° informed the fit, to avoid a bias in the measurement of eccentricity that occurs near the border of the mapping stimulus [17] and near the foveal confluence. The residuals of the fit to the aggregate data (Fig. 3C) show increasing error as the template approaches 10° of eccentricity; below we demonstrate that bias in the empirical measurement of eccentricity is responsible for this deviation.

A leave-one-out analysis tested if unsmoothed retinotopic eccentricity could be predicted for individual subjects from their anatomy (Figure 3D). The error across subjects in specification of retinotopic eccentricity from anatomy is generally <1.0° but, as with the aggregate residual error (Fig. 3C), increases sharply beyond approximately 8° of template eccentricity (the median absolute and signed leave-one-out errors for all vertices in V1 with template values between 2.5° and 8° were 0.91° and 0.39°).

If measurement bias near the edge of the stimulus is responsible for the apparent template inaccuracy between 8–10° eccentricity, then the performance of the template in this range should be restored for data collected with more eccentric stimulation. We fit our model to the aggregate of subjects studied with a stimulus that extended to 20°, again excluding those points within 2° of the outer edge of the stimulus. We asked how well the cortical eccentricity function derived from these data would match that measured using the inner 8° of the 10° dataset. Figure 3E is a histogram of every vertex from every subject from the 10° study while Figure 3F plots all vertices from the 20° study. We find that the exponential cortical eccentricity functions fit to the two independent datasets are almost perfectly superimposed and that the spread of points seen near the stimulus border of the 10° dataset (Fig. 3E) has condensed.

Therefore, not only can cortical anatomy predict eccentricity organization with a median absolute error <1°, it is more accurate than measurement itself near the stimulus border.

Measurement error

A limit on the accuracy of template prediction is error in the measurement of visual field values for individual subjects. We examined the within-subject, median split-halves measurement error of eccentricity in the 10° dataset (Fig. 4) and found that it is only modestly lower (0.75°) than the median leave-one-out error of the anatomical template (0.91°). This comparison suggests that a substantial proportion of the residual error of the template can be attributed to measurement error in individual subjects; this error would persist even in the presence of a perfect template representation. The corresponding split-half analysis of polar angle (Fig. S3A, B) yielded similar results, with a median absolute error of 7.76°, compared to the template's leave-one-out error of 11.43°. The supplemental information considers other sources of variability, including anatomical registration and hemispheric differences (Fig. S2, Table S1).

To estimate the scan time needed to obtain retinotopic mapping with the same median absolute error as that of anatomical prediction, we collected 96 minutes of RM data for a single example subject (a 22 year old male with normal vision). Forty-eight minutes of data were compared to disjoint 16, 32, and 48 minute subsets of the scan, and the median absolute errors of each comparison was fit with a decaying exponential (Fig. S3D, E). We found ~25 minutes of retinotopic mapping data in this (arguably optimal) participant was needed to match the prediction performance of our template for polar angle in the other 19 subjects, and ~10 minutes of scanning to match the template eccentricity performance.

Discussion

Topographic maps are a common motif in the cortical organization of sensory information. Such maps have been observed in the tonotopic mapping of the primary auditory cortex [18–20] and the somatotopic mapping of the sensorimotor cortex [21–23]. A fundamental question is whether these maps develop in a systematic manner with respect to cortical structure. In the case of sensorimotor cortex, for example, a characteristic "knob" on the precentral gyrus is associated with the motor representation of the hand [24]. For the primary visual cortex, prior work has established the calcarine sulcus represents the horizontal azimuth [11]. We extend this finding by demonstrating that the polar angle and eccentricity representation of the visual world is tightly coupled to sulcal folding anatomy.

This regularity is captured within an algebraic template of the retinotopic map. The template fitting procedure is automatic, non-stochastic, and independent of user choices, such as anatomical landmarks. These features allow the ready comparison of retinotopy from individuals or populations while avoiding sources of human error.

The automated fit to V1 may also serve as a starting point for template fitting of higher-order visual areas. The Schira *et al.* model [8], upon which we based our template, extends lines of eccentricity and polar angle to surrounding visual areas, providing a ready mechanism for template extension. Another useful target is the foveal confluence, which is challenging to define by RM methods. Notably, data collected with higher spatial resolution [12] could be used to further refine our template within this region. The success of these extensions is both dependent upon and informative regarding the presence of subject variability in structure-function mapping beyond primary visual cortex. Examination of cytoarchitecture in cadaveric brains within an automated surface template has shown that higher-order cortical areas (e.g., V2, Broca's area) are more variable in location than primary areas such as V1 or primary sensory cortex [25]. Further improvements in anatomical registration may resolve this variability, although the automated software used here (FreeSurfer) already has accuracy comparable to human-guided, landmark-based alignment for the calcarine sulcus [26]. Alternatively, the extent of striate cortex may be defined by direct imaging of intracortical myelination [27], providing a still firmer basis for initial, between-subject alignment of area V1.

Practically, we have found that anatomical imaging alone can predict retinotopic arrangement with a precision that is comparable to 10–25 minutes of fMRI. The relative performance of anatomical prediction is doubtless better in populations less able to cooperate with maintaining the attention, gaze fixation, and head immobility required for functional mapping studies. Patients with ophthalmologic disease are an obvious target for the use of anatomically derived retinotopic maps.

Finally, our work may be regarded as the culmination of an enterprise started by Gordon Holmes in 1918, when he provided a map of the "cortical retina" by relating perimetric, visual field scotomas to the trajectory of missile wounds to the brain. The final diagram of his report offers a "probable representation of the different portions of the visual fields in the calcarine cortex". In the legend below this figure—remarkable for its timelessness given the crude technique he had available—Holmes cautions that "this diagram does not claim to be in any respect accurate; it is merely a schema". The atlas we have produced is a descendent of Holmes' effort but for which we can claim accuracy, and with known precision.

Experimental Procedures

Subjects and Stimuli

Twenty-five subjects with normal vision participated in fMRI scanning experiments (15 women, mean age 24, range 20–42). The study was approved by the University of Pennsylvania Institutional Review Board, and all subjects provided written informed consent.

Two primary datasets were collected. The first, 10° dataset (19 subjects), used a single sweeping bar of 2.5° thickness which flickered at 5 Hz [9]. The bar traveled 1.25° every 3 s within a central 20° aperture in 4 orientations (horizontal, vertical, oblique +45°, oblique −45°) over 27 minutes while subjects maintained central fixation. For the second, 20° dataset (6 subjects), subjects fixated on the the left or right edge of the screen each for 64 minutes while standard "ring and wedge" stimuli [15] swept in the periphery in 16 steps.

Magnetic Resonance Imaging

Whole-brain BOLD fMRI data (TR 3 s, 3 mm isotropic voxels) and a standard T1-weighted anatomical image (1 mm isotropic voxels) were acquired at 3-Tesla. Anatomical data were processed using the FMRIB Software Library (FSL) toolkit (http://www.fmrib.ox.ac.uk/fsl/) and individual subject brain surfaces reconstructed and inflated using FreeSurfer (v5.1)

(http://surfer.nmr.mgh.harvard.edu/) [10,30,31]. Individual hemispheric maps were registered to a common FreeSurfer template surface pseudo-hemisphere (fsaverage_sym) [7,32]. Probabilistic boundaries for V1 in the reconstructed brain surface for each subject were generated using atlas definitions [6].

Calculation of retinotopic mapping values

Initial statistical analysis used a finite-impulse-response (FIR) basis of shifted delta functions to model neural response to the stimulus positions. The BOLD signal was modeled with a population average hemodynamic response (HRF) [28] (for the 10° dataset) or with a subject-specific HRF derived from a separate, blocked visual stimulation scan (for the 20° dataset). Nuisance covariates included effects of scan, global signals, spikes (periods of raw signal deviation greater than two standard deviations from the mean), and cardiac and respiratory fluctuations from simultaneously recorded pulse-oximetry (when available) [29].

Polar angle and eccentricity values were defined either by the population receptive field (pRF) approach [9] (for the 10° dataset) or by identification of the peak of a Gaussian fit to the set of FIR β weights derived from the initial linear model analysis (for the 20° dataset).

Data aggregation and Template Fitting

Vertices from the predicted V1 region [6] were projected from 3D surface coordinates to a 2D map with a shear transformation applied to reduce spherical curvature in the embedding. Aggregate maps were constructed by taking the mean polar angle or eccentricity for each vertex position across all subjects with responses at that position. Vertices for which two or fewer subjects had significant BOLD responses or for which the standard deviation of responses was greater than 3.3° of eccentricity or 60° of polar angle were excluded from the aggregate fits due to low confidence.

An algebraic model was fit to the aggregate RM data within the 2D space. The boundaries of V1 were defined by an ellipse. Iso-eccentric bands within V1 followed hyperbolas that were orthogonal to the iso-angular bands, which were also ellipses (see Supplemental Experimental Procedures, and Fig. S1).

For fitting of the eccentricity model, all vertices whose eccentricity values were within 2° of the outer stimulus border were discarded to avoid previously described measurement bias at the stimulus edges [17], as were voxels whose responses were <2.5°. Fitting was performed using a nonlinear numeric log-error minimization technique on the spatially unsmoothed retinotopic data. For eccentricity, the template was exponential along iso-angular bands (i.e., eccentricity varied exponentially across iso-angular bands) using published starting parameters [5]. The template was given the form $r = 90°\exp(q(x - 1))$, where x is the coordinate of the iso-eccentric band passing through a particular point and q is the fit parameter. For polar angle, the template was polynomial with a starting parameter of 1. The template was given the form $\theta = 90° + 90° \operatorname{sgn}(y) |y|^q$, where y is the coordinate of the iso-angular band passing through a particular point and q is the fit parameter.

Supplementary Material

Refer to Web version on PubMed Central for supplementary material.

Acknowledgments

We thank G. Boynton for his thoughts regarding bias in measurement of eccentricity and to C. Broussard for developing the visual stimulation software. This work was supported by the Pennsylvania State CURE Grant, P30 EY001583 and P30 NS045839-08, and by NIH Grant 1 R01 EY020516-01A1.

References

1. Holmes G. Disturbances of visual orientation. Br J Ophthalmol. 1918; 2(9):449–468. [PubMed: 18167816]
2. Andrews TJ, Halpern SD, Purves D. Correlated size variations in human visual cortex, lateral geniculate nucleus, and optic tract. J Neurosci. 1997; 17(8):2859–2868. [PubMed: 9092607]
3. Dougherty RF, Koch VM, Brewer AA, Fischer B, Modersitzki J, Wandell BA. Visual field representations and locations of visual areas V1/2/3 in human visual cortex. J Vis. 2003; 3(10):586–598. [PubMed: 14640882]
4. Amunts K, Malikovic A, Mohlberg H, Schormann T, Zilles K. Brodmann's areas 17 and 18 brought into stereotaxic space-where and how variable? NeuroImage. 2000; 11(1):66–84. [PubMed: 10686118]
5. Qiu A, Rosenau BJ, Greenberg AS, Hurdal MK, Barta P, Yantis S, Miller MI. Estimating linear cortical magnification in human primary visual cortex via dynamic programming. NeuroImage. 2006; 31(1):125–138. [PubMed: 16469509]
6. Hinds OP, Rajendran N, Polimeni J, Augustinack J, Wiggins G, Wald L, Diana Rosas H, Potthast A, Schwartz El, Fischl B. Accurate prediction of V1 location from cortical folds in a surface coordinate system. NeuroImage. 2008; 39(4):1585–1599. [PubMed: 18055222]
7. Greve, D.; Sabuncu, M.; Buckner, R.; Fischl, B. Hum Brain Mapp. Quebec City, Canada: 2011. Automatic surface-based interhemispheric registration with FreeSurfer.
8. Schira MM, Tyler CW, Spehar B, Breakspear M. Modeling magnification and anisotropy in the primate foveal confluence. PLoS Comp Biol. 2010; 6(1):e1000651.
9. Dumoulin SO, Wandell BA. Population receptive field estimates in human visual cortex. NeuroImage. 2008; 39(2):647–660. [PubMed: 17977024]
10. Fischl B, Dale AM. Measuring the thickness of the human cerebral cortex from magnetic resonance images. Proc Natl Acad Sci USA. 2000; 97(20):11050–11055. [PubMed: 10984517]
11. Rajimehr R, Tootell RBH. Does retinotopy influence cortical folding in primate visual cortex? J Neurosci. 2009; 29(36):11149–11152. [PubMed: 19741121]
12. Schira MM, Christopher TW, Breakspear M, Spehar B. The foveal confluence in human visual cortex. J Neurosci. 2009; 29(28):9050–9058. [PubMed: 19605642]
13. Horton JC, Hoyt WF. The representation of the visual field in human striate cortex. A revision of the classic Holmes map. Arch Ophthalmol. 1991; 109(6):816–824. [PubMed: 2043069]
14. Sereno MI, Dale AM, Reppas JB, Kwong KK, Belliveau JW, Brady TJ, Rosen BR, Tootell RB. Borders of multiple visual areas in humans revealed by functional magnetic resonance imaging. Science. 1995; 268(5212):889–893. [PubMed: 7754376]
15. Engel SA, Glover GH, Wandell BA. Retinotopic organization in human visual cortex and the special precision of functional MRI. Cereb Cortex. 1997; 7(2):181–192. [PubMed: 9087826]
16. Duncan OD, Boynton GM. Cortical magnification within human primary visual cortex correlates with acuity thresholds. Neuron. 2003; 38(4):659–671. [PubMed: 12765616]
17. Baseler H, Alyssa BA, Sharpe LT, Morland AB, Jägle H, Wandell BA. Reorganization of human cortical maps caused by inherited photoreceptor abnormalities. Nat Neurosci. 2002; 5(4):364–370. [PubMed: 11914722]
18. Formisano E, Kim DS, Di Salle F, van de Moortele PF, Ugurbil K, Goebel R. Mirror-symmetric tonotopic maps in human primary auditory cortex. Neuron. 2003; 40(4):859–869. [PubMed: 14622588]
19. Humphries C, Liebenthal E, Binder JR. Tonotopic organization of human auditory cortex. NeuroImage. 2010; 50(3):1202–1211. [PubMed: 20096790]
20. Striem-Amit E, Hertz U, Amedi A. Extensive cochleotopic mapping of human auditory cortical fields obtained with phase-encoding FMRI. PLoS One. 2011; 6(3):e17832. [PubMed: 21448274]
21. Penfield W, Boldrey E. Somatic motor and sensory representation in the cerebral cortex of man as studied by electrical stimulation. Brain. 1937; 60(4):389–443.
22. Grafton ST, Woods RP, Mazziotta JC, Phelps ME. Somatotopic mapping of the primary motor cortex in humans: activation studies with cerebral blood flow and positron emission tomography. J Neurophysiol. 1991; 66(3):735–743. [PubMed: 1753284]

23. Rao SM, Binder JR, Hammeke TA, Bandettini PA, Bobholz JA, Frost JA, Myklebust BM, Jacobson RD, Hyde JS. Somatotopic mapping of the human primary motor cortex with functional magnetic resonance imaging. Neurology. 1995; 45(5):919–924. [PubMed: 7746407]
24. Yousry TA, Schmid UD, Alkadhi H, Schmidt D, Peraud A, Buettner A, Winkler P. Localization of the motor hand area to a knob on the precentral gyrus. A new landmark. Brain. 1997; 120(Pt 1): 141–157. [PubMed: 9055804]
25. Fischl B, Sereno MI, Tootell RB, Dale AM. High-resolution intersubject averaging and a coordinate system for the cortical surface. Hum Brain Mapp. 1999; 8(4):272–284. [PubMed: 10619420]
26. Pantazis D, Joshi A, Jiang J, Shattuck DW, Bernstein LE, Damasio H, Leahy RM. Comparison of landmark-based and automatic methods for cortical surface registration. NeuroImage. 2010; 49(3): 2479–2493. [PubMed: 19796696]
27. Trampel R, Ott DV, Turner R. Do the congenitally blind have a stria of Gennari? First intracortical insights in vivo. Cereb Cortex. 2011; 21(9):2075–2081. [PubMed: 21310782]
28. Aguirre GK, Zarahn E, D'esposito M. The variability of human, BOLD hemodynamic responses. NeuroImage. 1998; 8(4):360–369. [PubMed: 9811554]
29. Verstynen TD, Deshpande V. Using pulse oximetry to account for high and low frequency physiological artifacts in the BOLD signal. NeuroImage. 2011; 55(4):1633–1644.30. [PubMed: 21224001]
30. Dale AM, Fischl B, Sereno MI. Cortical surface-based analysis I. Segmentation and surface reconstruction. NeuroImage. 1999; 9(2):179–194. [PubMed: 9931268]
31. Salat DH, Buckner RL, Snyder AZ, Greve DN, Desikan RS, Busa E, Morris JC, Dale AM, Fischl B. Thinning of the cerebral cortex in aging. Cereb Cortex. 2004; 14(7):721–730. [PubMed: 15054051]
32. Fischl B, Sereno MI, Tootell RB, Dale AM. High-resolution intersubject averaging and a coordinate system for the cortical surface. Hum Brain Mapp. 1999; 8(4):272–284. [PubMed: 10619420]

Highlights

- The retinotopic organization of human V1 can be predicted from cortical surface anatomy alone with an accuracy equivalent to a 10–25 minute functional MRI study.
- Prediction and fitting of retinotopy may be made automatically and without human landmark definitions.
- Within the template space, the V1 cortex from the two hemispheres may be treated as separate individuals.

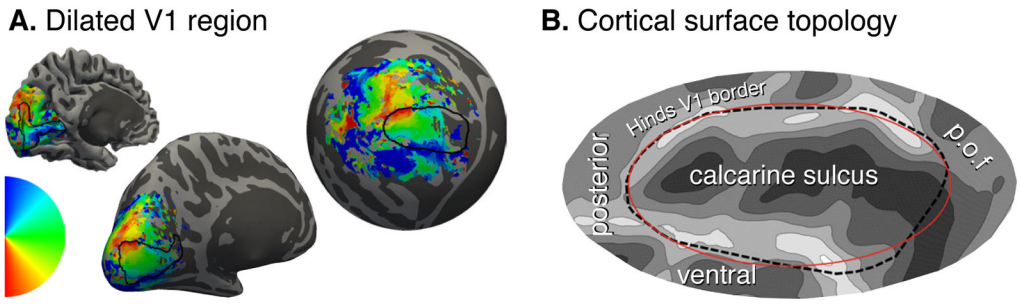

Fig. 1. Cortical surface atlas space

(A) Polar angle assignment is plotted on the folded (left), inflated (center), and spherical (right) hemisphere of a single subject. The black line shows the Hinds *et al.* [6] V1 outline throughout. (B) Cortical folding and landmarks around area V1. The calcarine sulcus, and parieto-occipital fissure (p.o.f.) are indicated. The red ellipse defines the border of the algebraic template. Fig. S1 illustrates the projection of the visual field onto this patch of cortex.

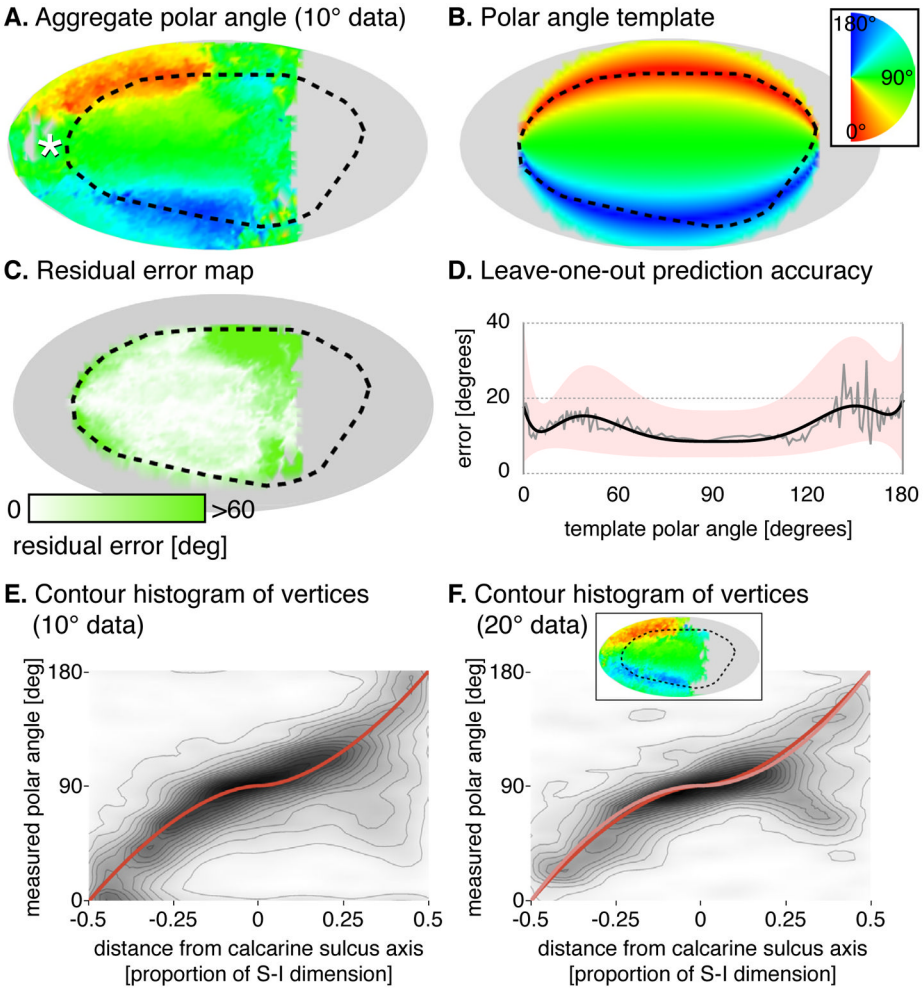

Fig. 2. Polar angle prediction

(A) Aggregate polar angle data of 18 of the 19 subjects shown visual stimuli within 10° of fixation (one significant outlier excluded). White asterisk is the foveal confluence; black dotted line is the Hinds *et al.* V1 border [6]. (B) Algebraic template, fit to the aggregate polar angle map. (C) Absolute residual error between the template fit and aggregate data. (D) Median absolute prediction error across vertices and subjects by template polar angle. The median error (grey), is fit by a fifth-order polynomial (black) with the similarly fit upper and lower quartiles defining the border of the pink region. (E) Contour histogram of all vertices from 10° dataset subjects, binned by measured polar angle and superior-inferior position in the template space. The template fit is shown in red. Each contour line corresponds to ~2,000 vertices. (F) Corresponding contour histogram from 20° dataset subjects. The template fit to the 20° dataset is in pink, and the fit to the 10° dataset is reproduced from Fig 2E in red. Each contour line corresponds to ~700 vertices. Inset is the aggregate map for the 20° dataset. Fig. S2A presents the polar angle aggregates and fits by hemisphere, and Table S1 provides the exact formulae measurements.

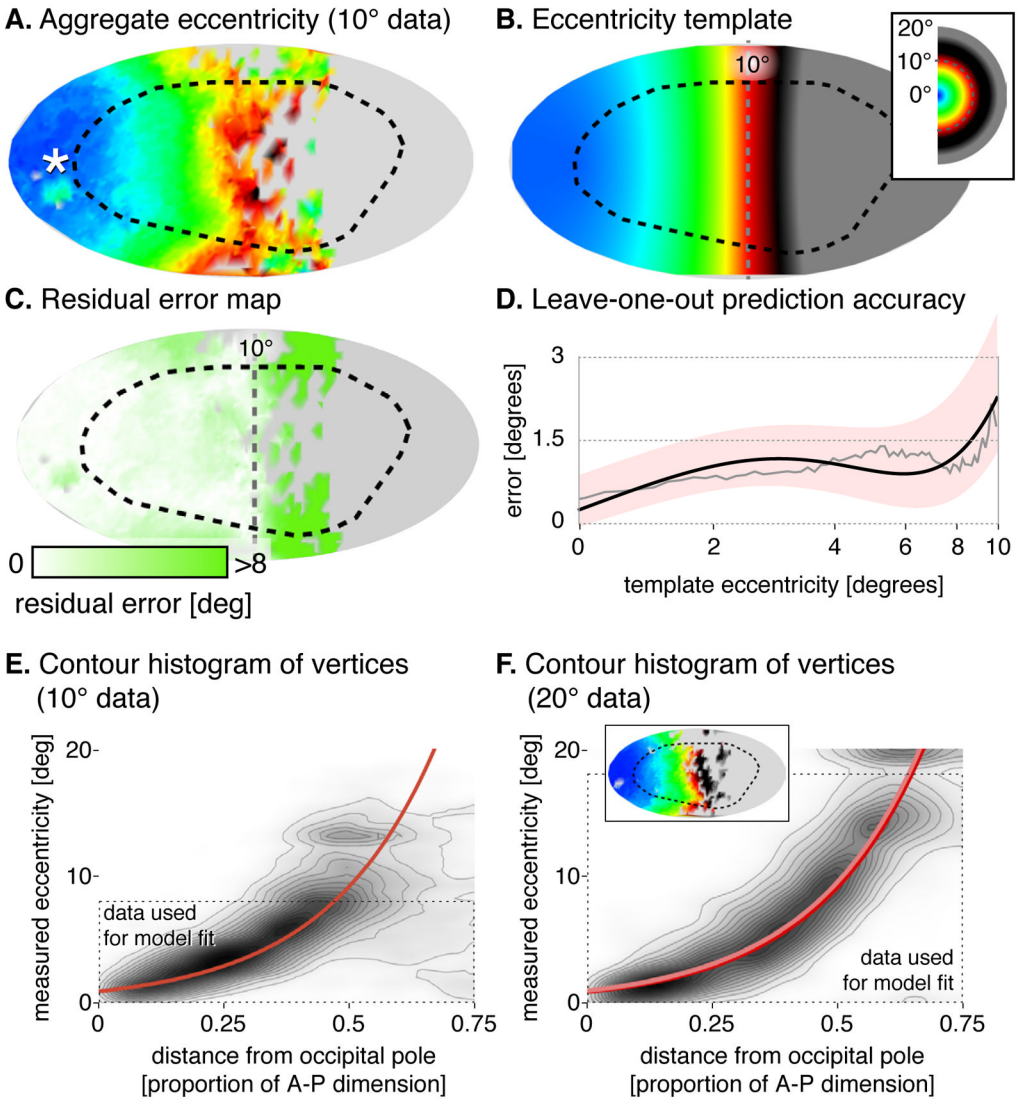

Fig. 3. Eccentricity prediction

(A) Aggregate eccentricity data of subjects (n = 19) shown visual stimuli within 10° of fixation. White asterisk is the foveal confluence; black dotted line is the Hinds *et al.* V1 border [6]. (B) Algebraic model, fit to the aggregate eccentricity map, after excluding those points with values ≤2.5° and ≥8°. (C) Absolute residual error between the template fit and aggregate data. (D) Median absolute prediction error across vertices and subjects by template eccentricity. The median error (grey), is fit by a fifth-order polynomial (black) with the similarly fit upper and lower quartiles defining the border of the pink region. (E) Contour histogram of all vertices from 10° dataset subjects, binned by measured eccentricity and posterior-anterior position in the template space. The exponential template fit is shown in red. Each contour line corresponds to ~2,000 vertices. (F) Corresponding contour histogram from 20° dataset subjects. The template fit to the 20° dataset is in pink, and the fit to the 10° dataset is reproduced from Fig 2E in red. Each contour line corresponds to ~800 vertices. Inset is the aggregate map for the 20° dataset. Fig. S2B presents the polar angle aggregates and fits by hemisphere, and Table S1 provides the exact formulae measurements.

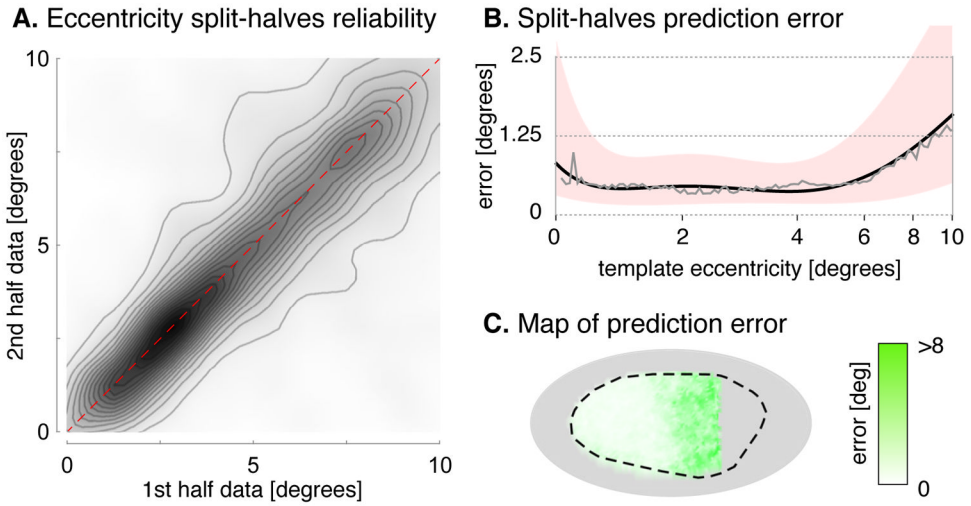

Fig. 4. Split-halves reliability of eccentricity

(A) A split-halves analysis plotted the eccentricity measured for each vertex for each subject from the first half of each ~30 minute scan against the eccentricity derived from the same vertex during the second half-scan. Each contour line corresponds to ~4,100 vertices (B) Median absolute split-halves error across vertices and subjects by template eccentricity. The median error (grey), is fit by a fifth-order polynomial (black) with the similarly fit upper and lower quartiles defining the border of the pink region. (C) Test-retest absolute residuals between first- and second-half measurements for each vertex shown on the cortical surface. Fig. S3 presents the corresponding measurements for polar angle.